Volume 257, number 1, 149–154 FEB 07738 October 1989

Solution conformation of endothelin determined by nuclear magnetic resonance and distance geometry

Satoshi Endo, Hiroshi Inooka, Yoshihiro Ishibashi, Chieko Kitada, Eiji Mizuta and Masahiko Fujino

Tsukuba Research Laboratories, Takeda Chemical Industries Ltd, 7 Wadai, Tsukuba, Ibaraki 300-42, Japan

Received 15 August 1989

The solution conformation of endothelium-derived vasoconstrictor peptide, endothelin, has been determined by two-dimensional ^{1}H-NMR spectroscopy and distance geometry. Conformation in the N-terminal core region (residues 1–15) is well-defined and a characteristic is the helix-like conformation in the segment from Lys^9 to Cys^{15}. Contrarily, the C-terminal tail region (residues 16–21) does not assume a defined conformation and there are no specific interactions between the core and the tail regions.

Endothelin; Vasoconstrictor peptide; Three-dimensional structure; NMR, ^{1}H; Distance geometry

1. INTRODUCTION

Endothelin (ET) is a 21-amino acid peptide initially isolated from the supernatant of cultured porcine endothelial cells, and has been shown to be one of the most potent vasoconstrictors known to date [1]. ETs have been identified in several mammals [2–4] and the homologous peptides, sarafotoxins, were found in the burrowing asp venom [5]. Characteristic of these peptides are the conserved two disulfide bridges and the hydrophobic C-terminal amino acid residues [6,7] (fig.1), which are considered to be important for the expression of its biological activities [8]. Synthetic truncated analogs of ET such as porcine $ET_{1-15}NH_2$ or porcine ET_{16-21} do not show vasoconstrictor activities [9] nor receptor binding activities [10]. Thus the overall tertiary structure of ET should be essential to its biological activities.

We are interested in the relation between powerful activities of ET and its 3D structure, but there have been no conformational studies reported.

In the present study, we report the determination of the 3D structure of ET in a DMSO-d_6 solution by the combined use of 2-dimensional ^{1}H-NMR spectroscopy and a distance geometry algorithm called DADAS [11,12]. Structures calculated from different initial conformations showed good agreement in the region, Cys^1–Cys^{15}, but agreement was poor in the following C-terminal segment, His^{16}–Trp^{21}. The determined structure will provide a basis for understanding the biological function of ET in terms of the 3D structure.

Correspondence address: S. Endo, Tsukuba Research Laboratories, Takeda Chemical Industries Ltd, 7 Wadai, Tsukuba, Ibaraki 300-42, Japan

Abbreviations: ET, endothelin; NMR, nuclear magnetic resonance; NOE, nuclear Overhauser enhancement; DMSO, dimethyl sulfoxide; RMSD, root mean square distance

2. MATERIALS AND METHODS

2.1. *Synthesis and purification of ET*

Endothelin was synthesized by the solution method and purified by column chromatography on Sephadex LH-20 followed by preparative HPLC. The purity of the final product was checked by analytical HPLC and amino acid analysis. The synthetic endothelin was indistinguishable from the natural product.

2.2. *NMR measurements and distance geometry calculations*

For the NMR experiments, approx. 5.5 mM solution of ET in DMSO-d_6 was prepared. A series of 2D spectra (DQF-COSY [13], HOHAHA [14], NOESY [15,16]) were recorded with 512 × 2048 data points on a Bruker AM-500 spectrometer at the probe temperature of 40°C. All the spectra were acquired in the phase sensitive mode using the TPPI procedure [17].

Three-dimensional structures were determined from the NMR data using the distance geometry program DADAS [11,12]. Proton-proton distance constraints as input data for DADAS were obtained from the analysis of NOESY spectrum. Additional constraints were obtained from the spin-spin coupling constants $J_{HN\alpha}$ measured by high-resolution DQF-COSY spectrum recorded with 512 × 8192 data points.

Distance geometry calculations were performed on a VAX 8530 computer using the program purchased from Jeol Trading Co. Ltd (Tokyo). Graphical representation and RMSD analysis of distance geometry structures were carried out on an Evans & Southerland PS 390 color graphics system interfaced to a VAX 8530 using the molecular graphics program BIOGRAF (BioDesign, Inc., Pasadena).

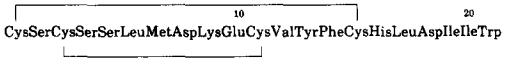

Fig.1. Amino acid sequence of human Endothelin I (ET-I) [4].

Published by Elsevier Science Publishers B.V. (Biomedical Division)
00145793/89/$3.50

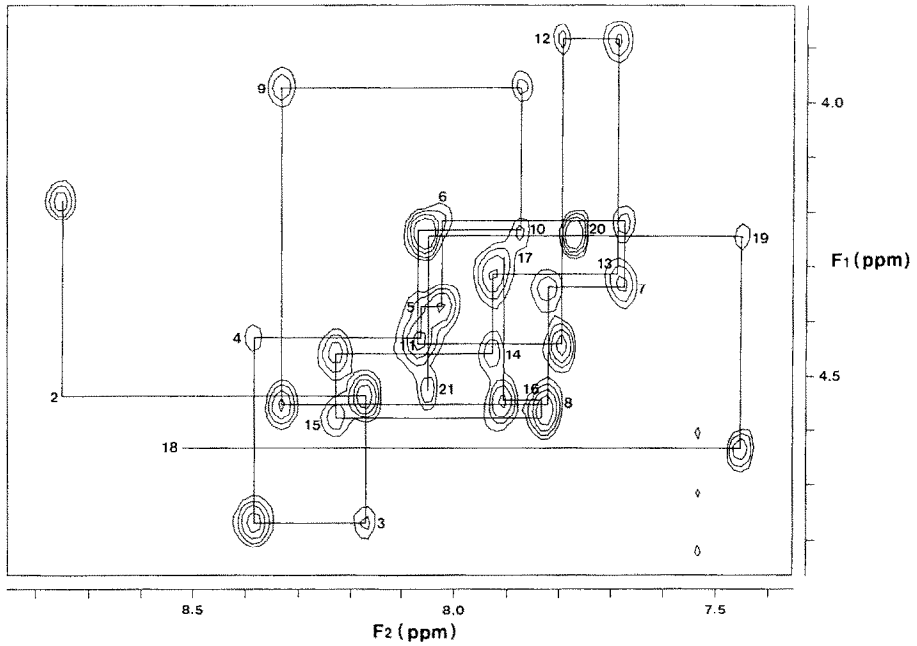

Fig.2. $C^{\alpha}H$-NH region of the NOESY spectrum (τ_m = 200 ms) of endothelin. The position of $C^{\alpha}H$-NH cross-peak of each residue is indicated by residue number and sequential connectivities are represented by solid lines.

3. RESULTS

Complete sequence-specific ^{1}H-NMR assignments were carried out by the analyses of DQF-COSY, HOHAHA and NOESY spectra. Fig.2 shows a part of NOESY spectrum with sequential connectivities. Chemical shifts of assigned resonances are listed in table 1. Fig.3 shows the summary of the observed sequential and long-range NOE connectivities [11].

Proton-proton distance constraints were obtained from the analysis of cross-peak intensities of NOESY spectrum with a mixing time of 200 ms. The possibility of spin diffusion effect was eliminated by consulting the NOE build-up curve obtained by NOESY experiments with various mixing times (50, 100, 150, 200, 300, 500 ms). Observed NOE intensities were converted into proton-proton distances using the $1/r^6$ relationship of NOE and fixed distances between β-methylene protons. Observed NOEs were classified into 4 groups according to their intensities and the upper bound for distance constraints of 2.3, 2.5, 3.0 and 4.0 Å was assigned, respectively. For intra-residue distances between amide- and α-protons, additional constraints were derived from spin-spin coupling constants, $J_{HN\alpha}$; thus more elaborate constraints were attributed. Intra-residue distance $d_{N\alpha}(i,i)$ is confined in the range 2.16 Å $\leqq d \leqq$ 2.85 Å [18]. In addition, for L-amino acids, $d_{N\alpha}$ cannot take on values between 2.2 Å and 2.6 Å because of steric hindrance [11]. NOE data did not show any distance $d_{N\alpha}(i,i)$ shorter than 2.2 Å so all $d_{N\alpha}$ were assumed to be longer than 2.6 Å. In case of $J_{HN\alpha} \geqq$ 8.0 Hz, lower bound and upper bound of distance constraints for corresponding $d_{N\alpha}$ was set to 2.8 Å and 2.9 Å, respectively. In other cases, the same lower bound of 2.6 Å and upper bound of 2.7 Å or 2.8 Å was assigned according to the NOE intensities. The information of the disulfide bridge was also included in the input data.

The number of distance constraints used as input data for DADAS calculations were as follows: 86 intra-residual, 46 sequential, and 25 medium- and long-range constraints. Calculations were started with 60 different randomly generated initial conformations. In order to save computing time, non-convergent structures were

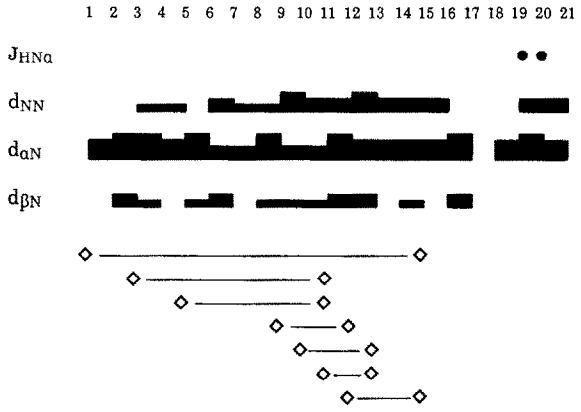

Fig.3. Summary of the observed NOE connectivities. Residues with $J_{HN\alpha} \geqq$ 8.0 Hz are indicated by closed circles (●). Terms d_{NN}, $d_{\alpha N}$, and $d_{\beta N}$ represent the sequential backbone connectivities with the usual meaning [11]. Intensities of the observed NOEs are classified into 4 levels represented by the thickness of the lines. Medium- and long-range connectivities are also indicated (◇——◇).

Table 1

Chemical shifts of proton resonances of human endothelin at 40°C in dimethylsulfoxide-d_6

Residue	Chemical shift (ppm)			
	NH	αH	βH	Others
Cys[1]	–	4.18	3.02,3.13	
Ser[2]	8.74	4.53	3.63,3.63	
Cys[3]	8.17	4.76	2.85,3.17	
Ser[4]	8.38	4.43	3.59,3.71	
Ser[5]	8.06	4.37	3.56,3.71	
Leu[6]	8.02	4.22	1.50,1.50	γCH 1.62 δHC$_3$ 0.84,0.89
Met[7]	7.67	4.34	1.85,2.02	γCH$_2$ 2.40,2.52 ϵCH$_3$ 2.04
Asp[8]	7.82	4.54	2.71,2.94	
Lys[9]	8.33	3.97	1.71,1.71	γCH$_2$ 1.39,1.39 δCH$_2$ 1.57,1.57 ϵCH$_2$ 2.70,2.70 ϵNH$_3$ 7.70
Glu[10]	7.87	4.23	1.91,2.04	γCH$_2$ 2.32,2.38
Cys[11]	8.07	4.44	2.96,3.05	
Val[12]	7.79	3.88	1.96	γCH$_3$ 0.75,0.80
Tyr[13]	7.68	4.32	2.70,2.81	2,6H 6.88 3,5H 6.58
Phe[14]	7.93	4.45	2.92,3.11	2,6H 7.29 4H 7.29 3,5H 7.20
Cys[15]	8.23	4.57	2.99,3.14	
His[16]	7.83	4.54	3.01,3.11	2H 7.93 4H 7.16
Leu[17]	7.90	4.28	1.49,1.49	γCH 1.61 δCH$_3$ 0.82,0.85
Asp[18]	8.52	4.63	2.50,2.76	
Ile[19]	7.45	4.24	1.71	γCH$_2$ 1.01,1.39 γCH$_3$ 0.76 δCH$_3$ 0.76
Ile[20]	7.77	4.24	1.74	γCH$_2$ 1.06,1.42 γCH$_3$ 0.81 δCH$_3$ 0.80
Trp[21]	8.05	4.52	3.05,3.15	2H 7.14 4H 7.53 5H 6.99 6H 7.07 7H 7.34 NH 10.76

Chemical shifts are indirectly referenced to internal DSS by the measurement of the residual methyl resonance of DMSO (2.52 ppm at 40°C)

abandoned at the beginning stage of DADAS calculation and only 30 structures were brought to the final stage of calculation. By considering the violation of the input constraints for each resulting structure, structures with the 5 smallest violations were chosen. Table 2 shows the root mean square distance (RMSD) values between all pairs among the 5 structures. When other structures are superposed on structure 2, average RMSD value is smallest and is 1.88 Å for main-chain atoms and 4.03 Å for all atoms.

Those analyses based on RMSD should be useful in estimating the overall convergency of the final structures but the extent of the coincidence of local conformations is difficult to estimate by such analyses. In order to investigate the local conformations of the final structures, we determined the distribution of each dihedral angle [19] among the 5 structures and the results are listed in table 3 along with values among the corresponding 5 initial conformations. From table 3 it is clear that main-chain conformation in the region Cys[1]–Cys[15] is well converged but that the C-terminal His[16]–Trp[21] region is disordered. Based on this observation, RMSD values only for the region Cys[1]–Cys[15] were calculated and are listed in table 2 in parentheses. Fig.4 shows the polypeptide backbones of the 5 structures superposed so as to minimize the RMSD value in the region Cys[1]–Cys[15]. It is clearly seen that the region Cys[1]–Cys[15] shows a good coincidence while the following C-terminal region does not assume a defined orientation relative to the preceding region.

Table 2

RMSD between 5 structures calculated by distance geometry

Structure	1	2	3	4	5
1	–	2.00 (1.65)	3.70 (2.01)	6.22 (1.32)	5.29 (1.32)
2	0.85 (0.49)	–	3.10 (1.68)	5.79 (1.98)	5.23 (1.90)
3	2.40 (0.31)	1.86 (0.58)	–	4.83 (2.17)	4.65 (2.21)
4	3.99 (0.85)	2.21 (0.48)	2.21 (0.48)	–	3.93 (1.28)
5	2.88 (0.31)	2.60 (0.48)	2.19 (0.29)	2.52 (0.76)	–

Root mean square distances (in Å) for main-chain atoms (lower left triangle) and for all atoms (upper right triangle). Values in parentheses are only those for the region Cys[1]–Cys[15]

4. DISCUSSION

In this study we have determined the solution conformation of ET by 2-dimensional ^{1}H-NMR spectroscopy and distance geometry.

ET is composed of the disulfide-linked 'core' portion, Cys[1]–Cys[15], and the C-terminal 'tail', His[16]–Trp[21]. Fig.4 shows the superposition of the 5 structures calculated from different initial conformations. The average RMSD value in the core region is 0.46 Å for main-chain atoms, which indicates a good convergence in this region. One of the important conclusions revealed here is the lack of specific interactions between the core and the tail, and another is the characteristic helix-like conformation in the region from Lys[9] to Cys[15]. As shown in fig.3, strong d_{NN} connectivities were observed in the segment from Lys[9] to His[16], along with some $d_{\alpha\beta}(i,i+3)$ connectivities, which suggested the existence of an α-helix here [11]. But the appearance of stronger $d_{\alpha N}(12,13)$ connectivity and continuous strong $d_{\alpha N}$ connectivities from Val[12] to His[16] cannot be reconciled with the α-helix [11]. Moreover temperature dependencies of amide proton chemical shifts did not show the presence of the hydrogen bonds in that region (data not shown). So it is concluded that the characteristic helix-like conformation in the region from Lys[9] to Cys[15] is not a regular α-helix.

As described in section 3, we have selected the initial conformations at the beginning stage of DADAS calculations. This may lead to a biased selection of initial conformations. In order to exclude this possibility, we analyzed the distribution of the dihedral angles among the 5 initial conformations (table 3). Table 3 shows that dihedral angle variations are quite large even in the well-converged region and that the aforementioned possibility was not the case. We also analyzed the dihedral angles of the final structures. It

is clearly seen that ϕ and ψ angles of residues from Ser[2] to Cys[15] show fairly good convergence. On the other hand, ϕ and ψ angles of His[16] to Asp[18] are poorly converged. This is the reason why the C-terminal segment did not show a defined orientation relative to the core portion (fig.4). It is interesting that ϕ and ψ angles of Ile[19] and Ile[20] are again well-defined. This may be a consequence of intra-residue and sequential distance constraints. Dihedral angles beyond χ^1 are poorly defined throughout the molecule. This is partly because resonances of prochiral groups were not stereospecifically assigned [20] and partly because the number of NOEs involving side-chain protons were not so many.

Kimura et al. [8] reported that the vasoconstrictor activity of ET is considerably decreased by the removal of the C-terminal Trp[21] residue. Our investigation showed that the C-terminal segment does not assume a defined conformation. This suggests that the C-terminal segment exhibits a considerable flexibility in solution, which is supported by the fact that resonances of Ile[19], Ile[20] and Trp[21] are substantially sharper than those of other residues (data not shown). It is unlikely, therefore, that removal of Trp[21] causes a considerable conformational change over the molecule leading to loss in activity; rather Trp[21] itself would be recognized by the receptor.

Neither ET_{1-15} nor ET_{16-21}, truncated derivatives of

Table 3

Dihedral angles and their variations among the 5 DADAS structures

Residue	ϕ	ψ	χ^1	χ^2	χ^3
Cys[1]	−157 ± 128	127 ± 59	−111 ± 91		
	(−20 ± 127)	(137 ± 107)	(−120 ± 102)		
Ser[2]	−37 ± 97	104 ± 7	−10 ± 64	−137 ± 90	
	(−82 ± 93)	(152 ± 75)	(−32 ± 80)	(−123 ± 104)	
Cys[3]	162 ± 2	112 ± 13	−106 ± 5		
	(−26 ± 101)	(104 ± 125)	(−149 ± 91)		
Ser[4]	−137 ± 12	98 ± 14	−56 ± 83	171 ± 103	
	(−145 ± 124)	(−74 ± 109)	(30 ± 107)	(175 ± 111)	
Ser[5]	−117 ± 20	119 ± 10	170 ± 109	−18 ± 114	
	(37 ± 86)	(176 ± 121)	(−77 ± 112)	(−17 ± 115)	
Leu[6]	−93 ± 0	29 ± 1	−78 ± 0	173 ± 2	−111 ± 129
	(6 ± 100)	(54 ± 94)	(−98 ± 94)	(−57 ± 67)	(33 ± 95)
Met[7]	118 ± 17	61 ± 11	−13 ± 88	−173 ± 41	112 ± 41
	(−82 ± 91)	(112 ± 107)	(−143 ± 98)	(54 ± 105)	(77 ± 77)
Asp[8]	163 ± 6	141 ± 3	−113 ± 15	73 ± 107	
	(60 ± 108)	(106 ± 100)	(−88 ± 93)	(−80 ± 113)	
Lys[9]	−94 ± 1	32 ± 3	−56 ± 110	168 ± 30	−152 ± 81
	(103 ± 97)	(129 ± 101)	(5 ± 108)	(−92 ± 95)	(−31 ± 97)
Glu[10]	−111 ± 4	−12 ± 5	164 ± 81	−168 ± 86	39 ± 75
	(−165 ± 117)	(62 ± 87)	(37 ± 91)	(−79 ± 107)	(27 ± 86)
Cys[11]	−151 ± 7	32 ± 2	−104 ± 8		
	(64 ± 125)	(155 ± 96)	(65 ± 91)		
Val[12]	−153 ± 2	23 ± 1	100 ± 1	28 ± 61	−159 ± 105
	(103 ± 111)	(63 ± 99)	(137 ± 110)	(4 ± 99)	(−111 ± 82)
Tyr[13]	−143 ± 3	54 ± 1	−174 ± 2	−44 ± 87	−94 ± 128
	(−11 ± 104)	(−72 ± 112)	(135 ± 107)	(138 ± 125)	(−97 ± 126)
Phe[14]	178 ± 0	64 ± 1	−145 ± 0	140 ± 98	
	(−32 ± 123)	(19 ± 130)	(93 ± 57)	(144 ± 100)	
Cys[15]	−155 ± 9	68 ± 2	−170 ± 8		
	(148 ± 109)	(39 ± 125)	(−55 ± 116)		
His[16]	−119 ± 78	127 ± 18	−45 ± 72	6 ± 92	
	(154 ± 87)	(−40 ± 117)	(−117 ± 100)	(17 ± 123)	
Leu[17]	−94 ± 53	−169 ± 81	6 ± 72	70 ± 114	−96 ± 82
	(109 ± 102)	(−174 ± 124)	(−71 ± 118)	(48 ± 90)	(−107 ± 89)
Asp[18]	−65 ± 109	98 ± 19	−119 ± 73	−115 ± 121	
	(121 ± 124)	(16 ± 87)	(−140 ± 93)	(−115 ± 121)	
Ile[19]	−155 ± 4	73 ± 3	−71 ± 8	131 ± 103	−160 ± 102
	(120 ± 57)	(163 ± 62)	(134 ± 118)	(118 ± 104)	(−9 ± 110)
Ile[20]	−143 ± 7	62 ± 4	−99 ± 58	109 ± 45	−166 ± 109
	(40 ± 119)	(−112 ± 120)	(104 ± 65)	(126 ± 79)	(70 ± 121)
Trp[21]	−128 ± 65	9 ± 112	−117 ± 38	1 ± 115	
	(155 ± 80)	(19 ± 102)	(−62 ± 97)	(−170 ± 67)	

For each angle the range of values covered by the 5 DADAS structures is represented by the center of the range and its size. Values in parentheses are those for the corresponding initial conformations

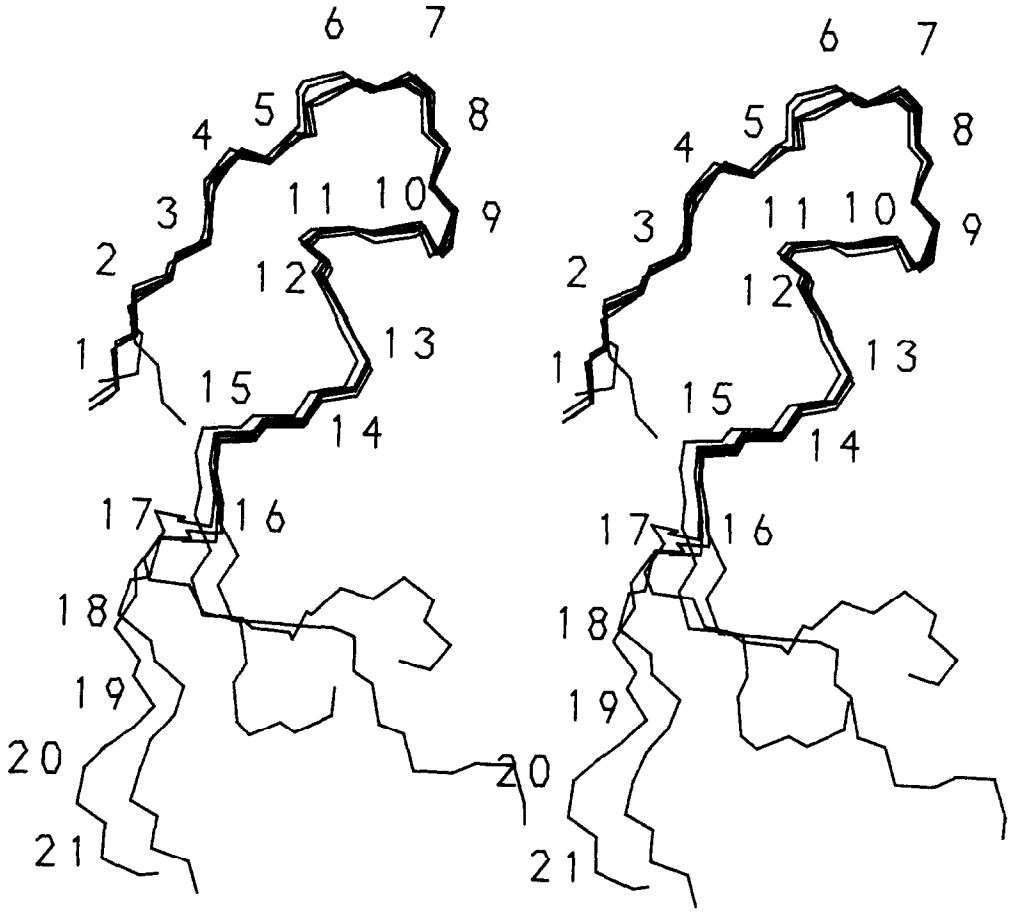

Fig.4. Stereo-view of the five DADAS structures superposed so as to minimize the RMSD of the backbone atoms, N, C and C′, in the region Cys^{1}–Cys^{15}.

ET, shows constricting activity and receptor binding activity [9,10]. These observations suggest that the receptor for ET recognizes an 'active conformation' consisting of both the core and the tail portion. Our results, however, do not show the interaction between the core and the tail portions in solution, so it seems that the receptor-bound conformation of ET is different from that in solution. The presence of the hydrophobic tail suggests the importance of the hydrophobic interaction on the receptor. Conformational analyses in systems other than solution, say, in the lipid bilayer, will be helpful for the better understanding of the structure-activity relationship of ET.

REFERENCES

[1] Yanagisawa, M., Kurihara, H., Kimura, S., Tomobe, Y., Kobayashi, M., Mitsui, Y., Yazaki, Y., Goto, K. and Masaki, T. (1988) Nature 332, 411–415.

[2] Yanagisawa, M., Inoue, A., Ishikawa, T., Kasuya, Y., Kimura, S., Kumagaye, S., Nakajima, K., Watanabe, T.X., Sakakibara, S. and Masaki, T. (1988) Proc. Natl. Acad. Sci. USA 85, 6964–6967.

[3] Itoh, Y., Yanagisawa, M., Ohkubo, S., Kimura, C., Kosaka, T., Inoue, A., Ishida, N., Mitui, Y., Onda, H., Fujino, M. and Masaki, T. (1988) FEBS Lett. 231, 440–444.

[4] Inoue, A., Yanagisawa, M., Kimura, S., Miyauchi, T., Goto, K. and Masaki, T. (1989) Proc. Natl. Acad. Sci. USA 86, 2863–2867.

[5] Takasaki, C., Tamiya, N., Bdolah, A., Wollberg, Z. and Kochva, E. (1988) Toxicon 26, 543–548.

[6] Lee, C.Y. and Chiappinelli, V.A. (1988) Nature 355, 303.

[7] Takasaki, C., Yanagisawa, M., Kimura, S., Goto, K. and Masaki, T. (1988) Nature 355, 303.

[8] Kimura, S., Kasuya, Y., Sawamura, T., Shinmi, O., Sugita, Y., Yanagisawa, M., Goto, K. and Masaki, T. (1988) Biochem. Biophys. Res. Commun. 156, 1181–1186.

[9] Kumagaye, S., Nakajima, K., Nishio, H., Kuroda, H., Watanabe, T.X., Kimura, T., Masaki, T. and Sakakibara, S. (1989) in: Peptide Chemistry 1988, pp.215–220, Protein Research Foundation, Osaka.

[10] Hirata, Y., Yoshimi, H., Emori, T., Shichiri, M., Marumo, F., Watanabe, T.X., Kumagaye, S., Nakajima, K., Kimura, T. and Sakakibara, S. (1989) Biochem. Biophys. Res. Commun. 160, 228–234.

[11] Wüthrich, K. (1986) NMR of Proteins and Nucleic Acids, Wiley, New York.

[12] Braun, W. and Go, N. (1985) J. Mol. Biol. 186, 611–626.

[13] Rance, M., Sørensen, O.W., Bodenhausen, G., Wagner, G., Ernst, R.R. and Wüthrich, K. (1983) Biochem. Biophys. Res. Commun. 117, 479–485.

[14] Bax, A. and Davis, D.G. (1985) J. Magn. Reson. 65, 355–360.
[15] Jeener, J., Meier, B.H., Bachmann, P. and Ernst, R.R. (1979) J. Chem. Phys. 71, 4546–4553.
[16] Macura, S., Huang, Y., Suter, D. and Ernst, R.R. (1981) J. Magn. Reson. 43, 259–281.
[17] Bodenhausen, G., Kogler, H. and Ernst, R.R. (1984) J. Magn. Reson. 58, 370–388.
[18] Wüthrich, K., Billeter, M. and Braun, W. (1983) J. Mol. Biol. 169, 949–961.
[19] Kline, A.D., Braun, W. and Wüthrich, K. (1988) J. Mol. Biol. 204, 675–724.
[20] Güntert, P., Braun, W., Billeter, M. and Wüthrich, K. (1989) J. Am. Chem. Soc. 111, 3997–4004.